OPEN ACCESS

University of BRISTOL

Peer reviewed version

Link to published version (if available):
10.1016/j.jphotobiol.2018.02.013

Link to publication record in Explore Bristol Research
PDF-document

University of Bristol - Explore Bristol Research
General rights

Bis(μ-chloro) bridged 1D Cu^I and Cu^{II} coordination polymer complex and mononuclear Cu^{II} complex: Synthesis, crystal structure and biological properties

Thangavel Thirunavukkarasu[a], Hazel A. Sparkes[b], Chandrasekar Balachandran[c], S. Awale[c], Karuppannan Natarajan[*d] and V. G. Gnanasoundari[a*]

[a]Department of Chemistry, CBM College, Coimbatore 641042, India.

[b]Department of Chemistry, University of Bristol, Cantock's Close, Bristol, BS8 1TS, UK.

[c]Division of Natural Drug Discovery, Institute of Natural Medicine, University of Toyama, 2630 Sugitani, Toyama 930-0194, Japan.

[d]Department of Chemistry, Bharathiar University, Coimbatore 641046, India.

Corresponding author e-mail: knatraj66@gmail.com

Abstract

A novel one-dimensional coordination polymer containing -Cu(I)-Cu(II)- core with chloro bridge on Cu(I) and ligand bridge on Cu(II) ions (**1**) and a mononuclear Cu(II) complex (**2**) have been synthesized from the reactions of 3- and 4-methoxy-3-quinolin-3-ylimino-methyl-2-phenol with [CuCl$_2$(PPh$_3$)$_2$]. The ligands and the complexes have been characterized by spectral and analytical methods. In addition, the structures of both the ligands and the copper complexes were confirmed by single crystal X-ray diffraction studies. In both complexes, the phenolic oxygen and azomethine nitrogen atom of the ligand coordinate to the copper ions in a monobasic bidentate manner resulting in an approximately square planar geometry around the copper ion. In the polymeric complex, the N atom of the quinoline ring is coordinated to Cu(I) in addition to the phenolic oxygen and azomethine nitrogen atom coordinating to Cu(II) ion, thus bridging Cu(I) and Cu(II) ions in the complex. The interactions of the compounds with calf thymus DNA (CT-DNA) have been followed by absorption and emission titration methods, which revealed that the compounds interact with CT-DNA through intercalation. Further, the interactions of the compounds with bovine serum albumin (BSA) were also investigated using UV–visible, fluorescence spectroscopic methods. The results indicated that complex **1** exhibited a stronger binding to CT-DNA and BSA than the free ligands and complex **2**. In addition, the *in vitro* cytotoxicity experiment showed that complexes **1** and **2** exhibit potent cytotoxic properties against PANC-1and Hela cells. Moreover, while complex **1** showed prominent cytotoxic activity against both PANC-1 and Hela cells with IC$_{50}$ of 17.91 and 11.67 μM, complex **2** showed

moderate cytotoxic activities with IC$_{50}$ of 25.13 and 16.41 μM in PANC-1 and Hela cells. Further, apoptosis was confirmed by fluorescence image using EB/AO reagent.

Introduction

Currently, there has been an increasing interest in the study of multinuclear copper complexes displaying quite interesting structural, magnetic, biological and catalytic properties [1]. In this connection, a large variety of synthetic strategies media have been applied to build such multinuclear architectures with different terminal and bridging ligands [2] and ligands of heterocyclic compounds containing a nitrogen atom have been given a special attention here [3–5]. As far as the area of bioinorganic chemistry research is concerned, focus has been given to the synthesis of new transition metal complexes possessing anticancer properties. Inorganic chemists concentrated on the strong interactions between the electron-rich biomolecules (DNA/protein) and electron-deficient metal ions in the complexes in order to ascertain the anticancer properties and hence, while designing new anticancer drugs, the study of the binding properties of metal complexes with DNA is of great significance [6]. It is also essential to find out the interaction of the complexes with protein since proteins in plasma have been found to carry several endo- and exo-genous compounds and therefore, in the process of developing new drugs, studies on the interaction of metal complexes with proteins like BSA are essential [7-10]. In the area of finding new metal based anticancer complexes, a combination of a heterocyclic ring with an azomethine moiety as lignds have been shown to exhibit potential biological activity [11–19]. Among the transition metal ions tried in the synthesis, copper ion has shown as promising candidate since its positive redox potential is ideal for biological electron transfer reactions [20]. In this connection, copper complexes containing heterocyclic compounds have shown a wide range of biological and pharmaceutical activities that includes DNA binding and cleavage, antimicrobial, anticancer and antioxidant behavior [21-24]. Due to the presence of heterocycles in quinolones, metal complexes derived from quinoline derivatives have been found to exhibit excellent DNA/protein binding and antitumor activities [25,26]. Our interest in the synthesis of polymeric complexes really emerged from the previous reports on the structural and biological applications of the Cu(II) coordination polymers (Figure A) [27-29]. Herein, we report

the synthesis, characterization and anticancer properties of a novel bridged one dimensional Cu(I)-Cu(II) coordination polymer complex and a mononuclear Cu(II) complex.
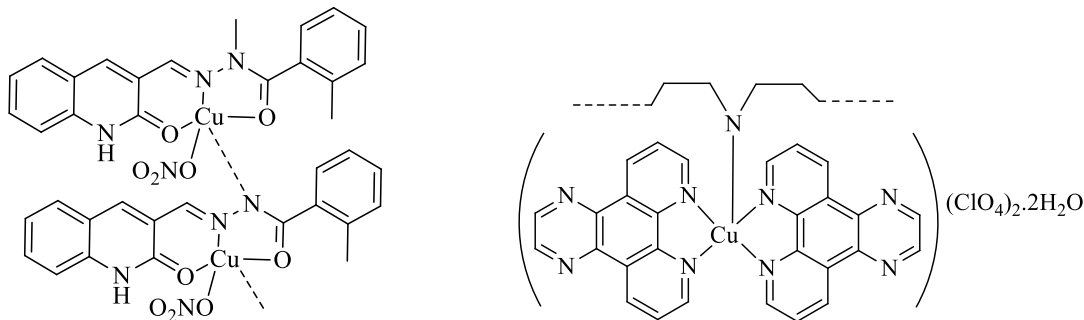

Figure A. Biologically active copper polymer complexes.

EXPERIMENTAL SECTION

Materials and method

All the chemicals used in the study were purchased from sigma Aldrich and used without further purification after having been dried according to the standard procedures [30]. The ligands and [CuCl$_2$(PPh$_3$)$_2$] were prepared according to the literature methods [31,32]. Infrared spectra of the ligand and the metal complexes were recorded as KBr discs over the range of 4000–400 cm^{-1} using a Jasco FT-IR 4100 FT-IR spectrophotometer. The melting points were recorded with a Lab India Melting point apparatus and elemental analyses (CHNS) were performed on a Vario EL III Elementar analyser instrument. The electronic spectra of the complexes were recorded with a Jasco V-630 spectrophotometer and emission spectra were measured using a Jasco FP 6600 spectrofluorometer. ^{1}H NMR spectra were recorded on a Bruker AMX 500 NMR spectrometer at 500 MHz. DNA binding, viscometry, Ethidium bromide replacement, Protein binding and cytotoxicity experiments were carried out by strictly following the procedures reported in the literature [33-37].

Crystallography

Single crystal X-ray diffraction data for the ligands **L₁** and **L₂**, and complexes **1** and **2** were collected at 100(2) K on a Bruker APEX II diffractometer using Mo-K$_\alpha$ radiation (λ = 0.71073 Å). Data collections were performed using a CCD area detector. Intensities were integrated in SAINT [38] and absorption corrections based on equivalent reflections were applied using SADABS [39]. The structures were solved using Superflip [40,41] and refined against F^2 in SHELXL [42,43] using Olex2 [44]. All of the non-hydrogen atoms were refined anisotropically while all the present hydrogen atoms were located geometrically and refined using a riding

model, apart from the O-H protons in **L₁** and **L₂** which were located in the difference map and refined freely. In the case of complex **1**, the toluene solvent included in the lattice was disordered over two positions; the occupancies of the fragments were determined by refining them against a free variable with the sum of the two sites set to equal 1, the occupancies were then fixed at the refined values. Restraints and constraints were applied to maintain sensible geometries and thermal parameters. In addition, Squeeze within Platon [45,46] was used to remove disordered solvent from the lattice of **L₁** that could not be sensibly modeled. Crystal structure and refinement data are given in Table 1. Crystallographic data for compounds have been deposited with the Cambridge Crystallographic Data Centre as supplementary publication CCDC 1468959, 1549578-1549580. Copies of the data can be obtained free of charge on application to CCDC, 12 Union Road, Cambridge CB2 1EZ, UK [fax(+44) 1223 336033, e-mail: deposit@ccdc.cam.ac.uk].

Preparation of the ligands

3-methoxy-3-quinolin-3-ylimino-methyl-2-phenol (L₁): **L₁** was prepared [31] using 3-amino quinoline (1.4 g 10mmol) and 2-hydroxy 3-methoxy benzaldehyde (1.5 g 10 mmol) as shown in Scheme 1. On cooling the mixture, an orange precipitate was formed which was filtered off. It was then washed with methanol and dried under *vacuum*. Orange colored single crystals suitable for X-ray diffraction studies were obtained from slow evaporation of the compound from ethyl acetate/methanol solvents. Yield: 96 %. M.p.: 156 ℃. Anal. Calc. for $C_{17}H_{14}N_2O_2$(%): C, 73.37; H, 5.07; N, 10.07. Found (%): C, 73.28; H, 4.95; N, 10.02; %. FT-IR (cm^{-1}) with KBr disk: 3428 (υ_{OH}), 1626 ($\upsilon_{C=N}$).UV-Vis (DMSO), λ_{max}(nm) [ε_{max} (dm^3 mol^{-1} cm^{-1})]:282 (78384), 331 (727414), 402 (444100) (Intra-ligand transition). ^{1}H NMR (300 MHz, CDCl₃) δ 13.26 (s, 1H, -OH), 8.96 (d, J = 2.4 Hz, 1H, (HC=N)), 8.83 (s, 1H, (aromatic)), 8.16 (d, J = 8.3 Hz, 1H, (aromatic)), 8.00 (d, J = 2.2 Hz, 1H, (aromatic)), 7.90 (d, J = 8.0 Hz, 1H, (aromatic)), 7.74 (t, J = 7.0 Hz, 1H, (aromatic)), 7.61 (t, J = 7.1 Hz, 1H, (aromatic)), 7.15 – 7.03 (m, 1H, (aromatic)), 6.96 (t, J = 7.8 Hz, 2H, (aromatic)), 3.98 (s, 3H, -OCH₃).

4-methoxy-3-quinolin-3-ylimino-methyl-2-phenol (L₂): **L₂** was prepared using 3-amino quinoline (1.4 g 10mmol) and of 2-hydroxy 4-methoxy benzaldehyde (1.4 g 10 mmol). The yellow compound obtained was separated and yellow colored single crystals suitable for X-ray diffraction studies were obtained from slow evaporation of the compound from chloroform/methanol. Yield: 89 %. M.p.: 158 ℃. Anal. Calc. for $C_{17}H_{14}N_2O_2$ (%): C, 73.37; H,

5.07; N, 10.07. Found (%): C, 73.29; H, 4.97; N, 10.01; %. FT-IR (cm^{-1}) with KBr disk: 3426 (υ_{OH}), 1628 ($\upsilon_{C=N}$). UV-Vis (DMSO), λ_{max}(nm) [ε_{max} (dm^3 mol^{-1} cm^{-1})]: 227 (65863), 358 (689) (Intra-ligand transition). ^{1}H NMR (DMSO-d$_6$, ppm): 13.245 (S, 1H, -OH), 9.1 (s, 1H, HC=N), 8.32 (d, J = 2.4 Hz, 1H, (aromatic)), 8.0 – 8.05 (m, 2H, (aromatic)), 7.72 – 7.16 (m, 2H, (aromatic)), 7.61 – 7.66 (m, 2H, (aromatic)), 6.55 (d, J = 4 Hz, 1H, (aromatic)), 6.60 – 6.63 (m, 1H, (aromatic)), 3.8 (s, 3H, -OCH$_3$),

Synthesis of the complexes

Complex 1: An ethanolic solution 10 (cm^3) of **L$_1$** (0.040 g 0.143 mmol) was slowly added to a solution of [CuCl$_2$(PPh$_3$)$_2$] (0.100 g 0.143 mmol) dissolved in chloroform (30 cm^3) and the mixture was heated under reflux for 6 h. Upon cooling, the resulting solution afforded a reddish brown colored precipitate which was filtered, washed with petroleum ether (60-80°C) and dried under *vacuum* before being recrystallized from hot methanol/toluene. The dark brown crystals obtained were suitable for X-ray diffraction. Yield: 48 %. M.p.:198 ^{o}C. Anal. Calc. for C$_{42}$H$_{36}$ClCu$_2$N$_2$O$_2$P (%): C, 68.60; H, 5.76; N, 12.00. Found (%): C, 68.57; H, 5.71; N, 11.96. FT-IR (cm^{-1}) with KBr disk: 1606 ($\upsilon_{C=N}$). UV-Vis (DMSO), λ_{max}(nm) [ε_{max} (dm^3 mol^{-1} cm^{-1})]: 225 (321679) (Intra-ligand transition), 272 (450282) (Intra-ligand transition), 400 (853267) (Ligand to metal charge transfer).EPR (X-band), 'g' value 2.04.

Complex (2): Complex **2** was prepared using the same procedure as described for complex **1** using **L$_2$** (0.040 g 0.143 mmol) and [CuCl$_2$(PPh$_3$)$_2$] (0.100 g 0.143 mmol). Upon cooling, the resulting solution afforded a reddish brown colored precipitate. It was filtered, washed with petroleum ether (60-80 ^{o}C) and dried under vacuum and recrystallized from hot methanol/DMF. The dark reddish brown crystals obtained were suitable for X-ray diffraction. Yield: 47 %. M.p.:176 ^{o}C. Anal. Calc. for C$_{34}$H$_{26}$CuN$_4$O$_4$ (%): C, 66.06; H, 4.24; N, 9.06. Found: C, 66.01; H, 4.18; N, 9.02; %. FT-IR (cm^{-1}) in KBr disk: 1593 ($\upsilon_{C=N}$). UV-Vis (DMSO), λ_{max}(nm) [ε_{max} (dm^{3}mol^{-1} cm^{-1})]:239 (959714) (Intra-ligand transition), 294 (696352) (Intra-ligand transition), 370 (333330) (Ligand to Metal Charge Transfer (LMCT).EPR (X-band), 'g' value 2.1.

Cytotoxic studies:

Using Dulbecco's modified Eagle medium (DMEM) containing 10 % fetal bovine serum and incubated in a humidified condition (5% of CO$_2$ and 95 % of air), the PANC-1 and Hela cells were cultured. Then, 10×10^5 cells/plate were seeded in the 96-well plate and incubated with fresh DMEM for 24 h. The cells were washed twice with phosphate-buffered saline (PBS) and freshly

prepared DMEM medium before the serially diluted test samples were added to the plate. The control and blanks were separated on each test plate. After 24 h of the treatment, the cells were washed twice with PBS and incubated with 100 μL of DMEM containing a 10 % WST-8 cell counting kit solution. It was then kept for 3-4 h of incubation and the absorbance was measured at 450 nm (PerkinElmer Enpiremultilabel reader). Cell viability was calculated by using the equation: Cell viability (%) = [Abs $_{(Test\ sample)}$ − Abs $_{(Blank)}$/ Abs $_{(Control)}$ − Abs $_{(Blank)}$]× 100 %

Fluorescence Images using EB/AO reagent

3×10^5 PANC-1 and Hela cells that were used for the study have been seeded in 30 mm dishes and were incubated overnight in humid conditions. The cells were then washed twice with PBS and freshly prepared serially diluted test samples in DMEM (treated) were added. After 24 h of incubation, 10 μL of ethidium bromide (EB)/acridine orange (AO) reagent was added to each tested dishes or control and incubated for another 5 min in dark condition. Then the cell morphology was captured by EVOS FL cell imaging system (20 × objective) under fluorescent mode.

Results and discussion

Synthesis

The reaction between [CuCl$_2$(PPh$_3$)$_2$] and the ligands in the ratio 1:1 in ethanol/chloroform resulted in the formation of new complexes as shown in **Scheme 1**.The ligands and complex **2** were soluble in methanol, ethanol, chloroform, dichloromethane, DMF and DMSO. Complex **1** was soluble in DMF and DMSO.
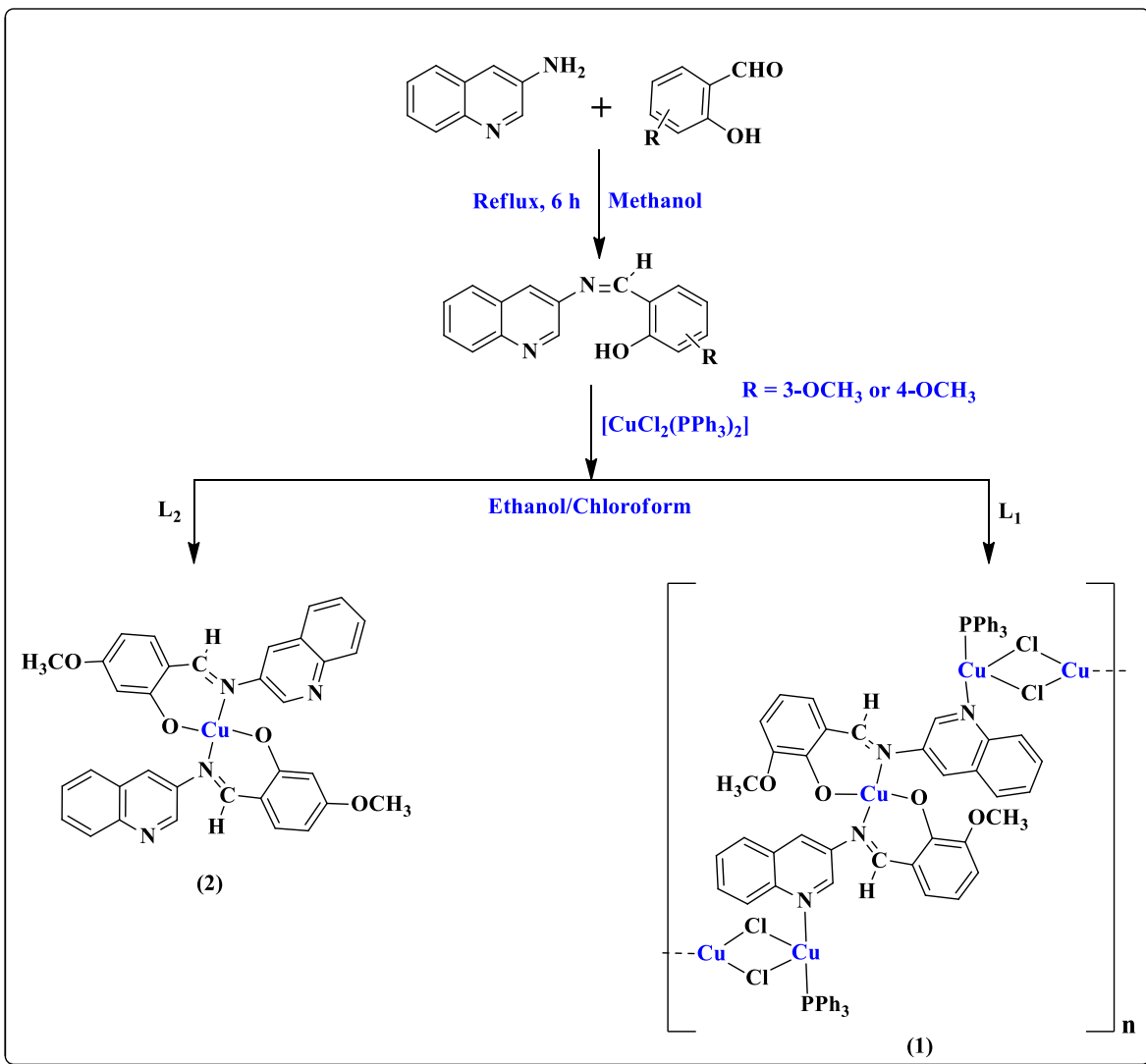
Scheme 1. Preparation routes of the ligands and their Cu(II) complexes.

Spectral characterization

The electronic spectra of the ligands showed three strong absorption bands in the regions at 227-282, 331-358 and 402 nm which have been assigned to intra ligand transitions [47]. In the Cu(II) complexes, three bands were observed in the regions at 239-255, 272-294 and 370-400 nm. The high intensity bands in the regions 239-255 and 272-294 nm have been assigned to intra ligand transitions, while the less intense band at 370-400 nm has been assigned as ligand to metal charge transfer transition [48-50]. The infrared spectra of the ligands exhibited -OH vibration in the region 3426-3428 cm^{-1} which disappeared completely after complexation with the Cu(II) ion as a result of the deprotonation followed by coordination through the phenolic oxygen in both the

two complexes. An azomethine nitrogen (HC=N) band that appeared in the region 1626-1628 cm^{-1} for the ligands has been shifted to lower frequency in the complexes as a result of coordination through the azomethine nitrogen [51]. In the ^1H NMR spectra, a sharp singlet appeared at δ 13.24–13.26 ppm was assigned to the phenolic -OH group in the free ligands (^1H NMR spectra of the ligands are shown in Figures S1and S2) which disappeared in the spectra of the complexes indicating the coordianation of phenolic O after deprotonation. The spectrum of **L₁** showed a doublet at δ 8.96 ppm for the azomethine proton while in **L₂** a singlet was observed at δ 9.1 ppm corresponding to the azomethine proton both of which disappeared on coordination to the metal ion in the complexes. However, the singlet found corresponding to the -OCH_3 group at δ 3.98–3.8 ppm for the ligands **L₁** and **L₂** were seen for the complexes as well. The resonances due to aromatic protons in the ligands were observed in the range at δ 8.63-6.63 ppm [52,53] and they were present for the complexes also. The X-band EPR of the Cu(II) complexes **1** and **2** were recorded at room temperature (Figure S3 and S4). Complex **1** showed well resolved quartet hyperfine splitting typical of square planar Cu(II) system. The observed values of g∥ and g⊥ were 2.34, 2.04 for complex **1** suggesting that the system is axial (g∥ > g⊥). The value of exchange interaction term G > 4.0 suggested that the unpaired electron of Cu(II) ion was present in the $dx^2\text{-}y^2$ orbital [54]. The complex **2** showed a well resolved isotropic resonance typical of square planar Cu(II) system. The g value of **2** was 2.1 [55].

Crystallography

The molecular structures of the ligands and complexes are shown in Figures 1-4, and the crystallographic data and structure refinement details are listed in Table 1. **L₁**crystallized in the orthorhombicspace group *Iba2* while **L₂** crystallized in a monoclinic crystal system with the space group *P2₁/c*. The azomethine, N2-C8, bond lengths of 1.288(6) Å (**L₁**) and 1.288 (2) Å(**L₂**) and the O2-C2 bond length of 1.348(6) Å (**L₁**) and 1.350 (2) Å(**L₂**) are indicative of the presence of a C=N double bond and a phenolic OH in both the ligands. Complex **1** crystallized in the triclinic space group *P*-1 as a 1D polymeric chain with two different Cu environments. One Cu (II) has two L₁ ligands coordinated in a bidentate fashion through the imine nitrogen (N1) and phenolic oxygen (O1) forming a six-member chelate rings. The Cu(II) ion adopts an approximately square planar geometry with unique O-Cu1-N angles of 88.85(7)° and 91.16(7)°. As the Cu(II) ion sits on an inversion center, it is therefore, necessarily in the same plane as the coordinated O and N from the two coordinated ligands. The charge on the complex was

neutralized by two oxygen ions from two ligand molecules. The quinolone nitrogen atom coordinated to a second Cu ion which has a distorted tetrahedral geometry with angles around the Cu ion ranging from 105.24(2)°–124.80(5)°. The second Cu ion also has a PPh$_3$ ligand attached and forms a double Cl bridge to a symmetry related Cu ion of the same type. Complex **2** crystallized in the monoclinic crystal system within the *P*2$_1$/*c* space group. Two L$_2$ coordinated in a bidentate manner to the Cu(II) ion through the imine nitrogen (N2) and phenolic oxygen (O1) forming six-member chelate rings and replacing all of the triphenylphospine ligands and chloride ions from the Cu(II) precursor which is rare. Again, the Cu(II) ion sits on an inversion center and adopts an approximately square planar geometry with unique O-Cu1-N angles of 89.75(5)° and 90.25(5)°. Important bond lengths and bond angles of the complexes **1** and **2** showed in (Table S1).
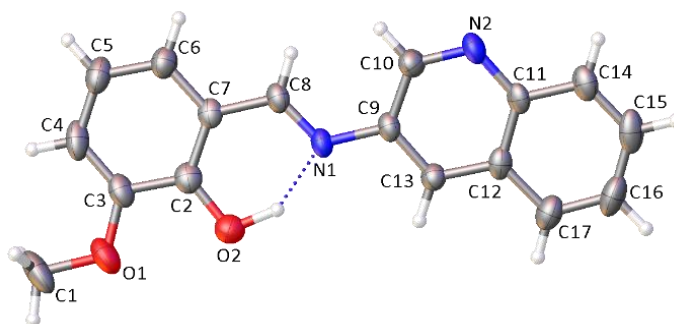

Figure 1. Structure of **L₁** with the atomic numbering scheme depicted. Thermal ellipsoids are depicted at the 50% probability level.
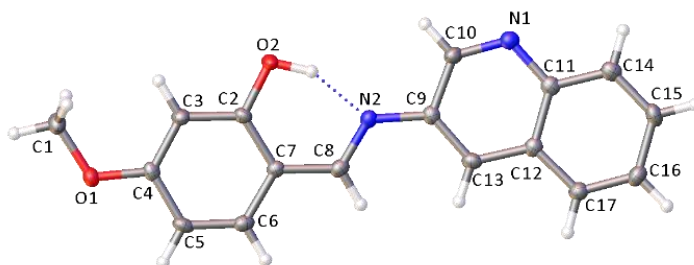

Figure 2. Structure of **L₂** with the atomic numbering scheme depicted. Thermal ellipsoids are depicted at the 50% probability level.
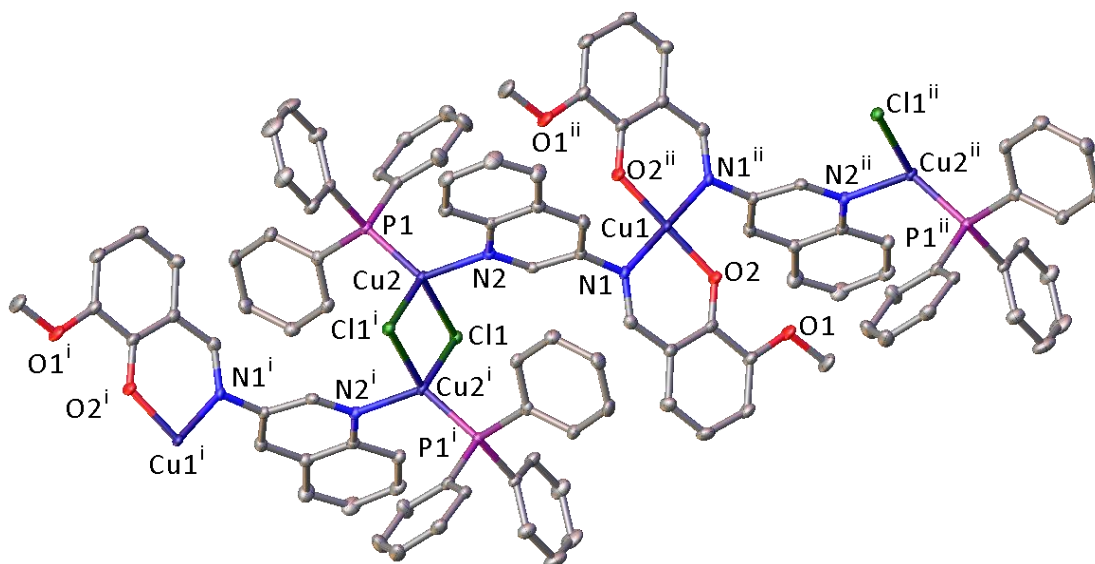
Figure 3. Structure of complex **1** with the atomic numbering scheme depicted. Thermal ellipsoids are depicted at the 50% probability level. Symmetry codes [i] = -*x*, 1-*y*, 2-*z*, [ii] = -*x*, 1-*y*, 1-*z*.
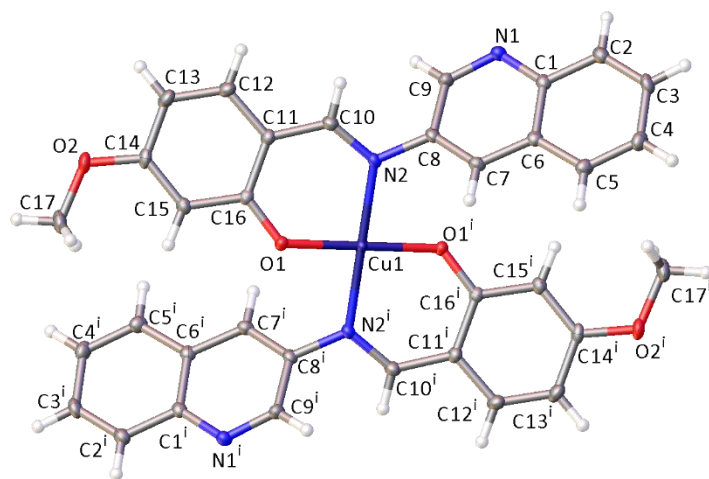

Figure 4. Structure of complex **2** with the atomic numbering scheme depicted. Thermal ellipsoids are depicted at the 50% probability level. Symmetry code [i] = 1-*x*, 1-*y*, 1-*z*.

Table 1. Crystal data and structure refinement data for **L₁**, **L₂**, complex **1** and **2**.

Identification code	**L₁**	**L₂**	**1**	**2**
Empirical formula	$C_{17}H_{14}N_2O_2$	$C_{17}H_{14}N_2O_2$	$C_{42}H_{36}ClCu_{1.5}N_2O_2P$	$C_{34}H_{26}CuN_4O_4$
Formula weight	278.30	278.30	762.46	618.13
Temperature/K	100(2)	100(2)	100(2)	100(2)
Crystal system	orthorhombic	monoclinic	triclinic	monoclinic
Space group	*Iba*2	*P*2₁/*c*	*P*-1	*P*2₁/*c*
a/Å	16.6220(13)	15.8477(9)	9.4952(2)	15.0224(5)
b/Å	30.172(3)	5.6667(3)	13.6296(3)	7.1743(2)
c/Å	6.2568(5)	15.5148(8)	14.2121(3)	12.9204(4)
α/°	90	90	84.202(2)	90
β/°	90	109.409(4)	76.260(2)	105.408(2)
γ/°	90	90	80.165(2)	90
Volume/Å³	3137.9(4)	1314.11(13)	1756.87(7)	1342.45(7)
Z	8	4	2	2
ρ_{calc}g/cm³	1.178	1.407	1.441	1.529
μ/mm⁻¹	0.079	0.094	1.078	0.863
F(000)	1168.0	584.0	787.0	638.0
Crystal size/mm³	$0.40 \times 0.24 \times 0.16$	$0.34 \times 0.18 \times 0.10$	$0.43 \times 0.29 \times 0.12$	$0.35 \times 0.33 \times 0.10$
Radiation	MoKα (λ = 0.71073)	MoKα (λ = 0.71073)	MoKα (λ = 0.71073)	MoKα (λ = 0.71073)
2θ range for data collection/°	4.902 to 52.744	2.724 to 55.826	4.104 to 55.922	2.812 to 55.966
Index ranges	-20 ≤ h ≤ 20, -37 ≤ k ≤ 36, -7 ≤ l ≤ 7	-20 ≤ h ≤ 20, -6 ≤ k ≤ 7, -20 ≤ l ≤ 20	-12 ≤ h ≤ 12, -17 ≤ k ≤ 15, -18 ≤ l ≤ 18	-19 ≤ h ≤ 19, -9 ≤ k ≤ 9, -11 ≤ l ≤ 17
Reflections collected	12314	11483	31217	12021
R_{int} / R_{sigma}	0.0807 / 0.0759	0.0658 / 0.0661	0.0492 / 0.0498	0.0307 / 0.0289
Data/restraints/parameters	3205/1/195	3149/0/195	8379/230/490	3235/0/197
Goodness-of-fit on F^2	0.994	1.010	1.026	1.035
Final R indexes [[I>=2σ (I)]	R₁ = 0.0613, wR₂ = 0.1324	R₁ = 0.0482, wR₂ = 0.1029	R₁ = 0.0373, wR₂ = 0.0820	R₁ = 0.0297, wR₂ = 0.0716
Final R indexes [all data]	R₁ = 0.1126, wR₂ = 0.1567	R₁ = 0.0985, wR₂ = 0.1243	R₁ = 0.0599, wR₂ = 0.0899	R₁ = 0.0373, wR₂ = 0.0751
Largest diff. peak/hole / e Å⁻³	0.23/-0.23	0.26/-0.27	0.48/-0.53	0.37/-0.32

DNA binding studies

Before estimating the antitumor activities of any new compound, the interaction between DNA and the newly synthesized compounds need to be examined and one of the most common ways

to investigate such interaction is to use the electronic absorption spectroscopy [56,57]. Hence, we measured the absorption spectra using a constant concentration (10 µM) of the synthesized new compounds with increasing concentrations of CT-DNA (0-100 µM) (Figure 5). The following spectral changes were observed on the incremental additions of DNA to the test compounds. The absorption bands (intra-ligand transitions) of the ligands L_1 and L_2 exhibited a hyperchromism with approximately a 4 and 5 nm wavelength shifts respectively. The absorption spectrum of complex **1** which consists of three resolved bands (intra ligand and ligand to metal charge transitions) showed a hyperchromism with a wavelength shift of 3 nm as the DNA concentration was increased. In the case of complex **2**, hyperchromism with a wavelength shift of 5 nm was observed on the addition of DNA. In addition to the above change, complex **2** showed an isosbestic point appearing at 293 nm suggesting that a chemical equilibrium exists between the DNA and complex **2**. These results indicate that the compounds bind to DNA *via* intercalation. In order to to compare the binding strengths of the compounds, their intrinsic binding constants (K_b) with CT-DNA were determined from the following equation.

$$[DNA]/[\varepsilon_a\text{-}\varepsilon_f] = [DNA] / [\varepsilon_b\text{-}\varepsilon_f] + 1/K_b[\ \varepsilon_b\text{-}\varepsilon_f]$$

where [DNA] is the concentration of DNA in base pairs, ε_a is the extinction coefficient of the compound at a given DNA concentration, ε_f is the extinction coefficient of the complex in free solution and ε_b is the extinction coefficient of the complex when completely bound to DNA.

A plot of $[DNA]/(\varepsilon_a\text{-}\varepsilon_f)$ *versus* [DNA] gave a slope and an intercept equivalent to $1/[\varepsilon_a\text{-}\varepsilon_f]$ and $1/K_b[\varepsilon_b\text{-}\varepsilon_f]$ respectively. The intrinsic binding constant K_b obtained for L_1, L_2, **1** and **2** are 0.5873 × 10^5, 0.5042× 10^5, 1.3494 × 10^5 and 0.8743 × $10^5 M^{-1}$ respectively which have been obtained from the ratio of the slope to the intercept in the plots of [DNA] (Figure 6). From the binding constant values, it is observed that complex **1** exhibited a better binding than complex **2** and the free ligands withCT-DNA, possibly due to intercalative mode [58]. These results indicate that the complex **1** penetrates more deeply into and stacks more strongly with the base pairs of the DNA than the other compounds tested.
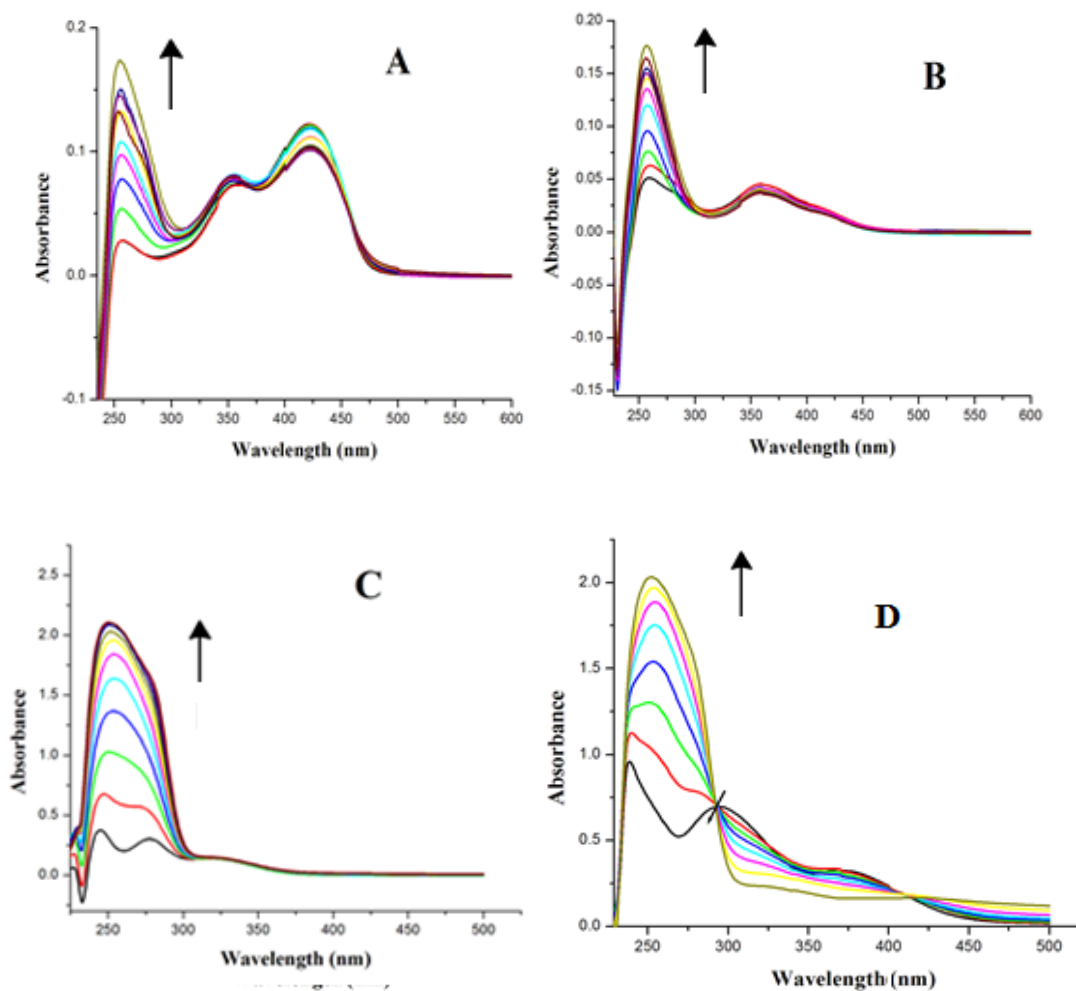
Figure 5. Electronic titration of the **L₁** (A), **L₂**(B), complex **1** (C) and complex **2** (D).Arrow shows that the absorption intensities increase upon increasing DNA concentration.
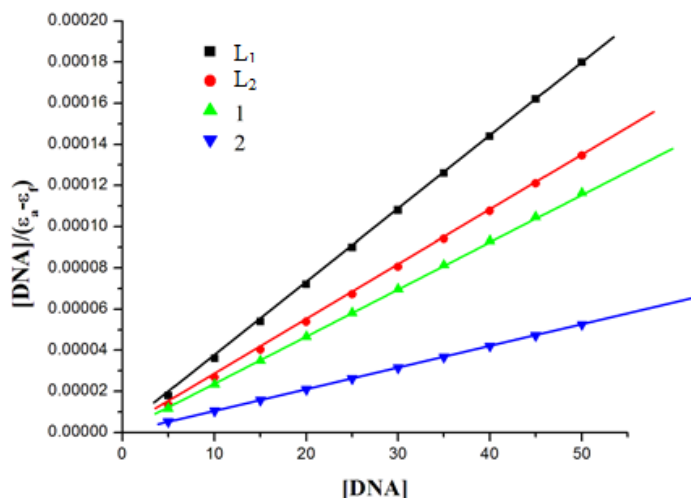
Figure 6. Plot of [DNA]/(ε_a-ε_f) *versus* [DNA] for the compounds.

Ethidium bromide (EB) replacement studies.

After having found the binding ability of compounds with DNA, some other studies are necessary to confirm the binding mode and the binding affinity and this is often done by ethidium bromide replacement investigations. Ethidium bromide (EB) is a planar cationic dye which can be used as a sensitive fluorescence probe for native DNA. Usually, EB emits an intense fluorescent light in the presence of DNA due to its intercalation between the adjacent DNA base pairs [59,60] which can be used indirectly as a proof to find out the DNA binding mode. There will be a decrease in fluorescence of EB as and when EB is replaced from DNA by a quencher, usually the compound under investigation and the consequent quenching is due to the reduction in the number of binding sites on the DNA that are still available to the EB. Hence, we carried out the emission spectra of the DNA-EB system with increasing concentrations of the ligands and the complexes and the results are shown in Figure 7. One can observe from the figure that there is a decrease in the fluorescence intensity due to the displacement of EB molecules from their DNA binding sites by the replacement by both the ligands and complexes [61].The extent of quenching of the compounds can be estimated qualitatively by employing Stern-Volmer equation:

$$I_0/I = 1 + Kq[Q].$$

Here, I_0 and I are the fluorescence intensities in the absence and presence of the compounds, Kq is a linear Stern–Volmer quenching constant, and [Q] is the total concentration of a compounds

to that of DNA. The Stern-Volmer plot is given in Figure 8 and the values of K_q have been obtained from the ratio of the slope to the intercept in the plot of I_0/I *versus* [Q]. The values obtained for the ligands and complexes are 2.90×10^3, 5.16×10^3, 4.04×10^3 and $5.22 \times 10^3 \, M^{-1}$ and these values indicate that the interaction of all of the compounds with DNA is likely to be through intercalation [62].
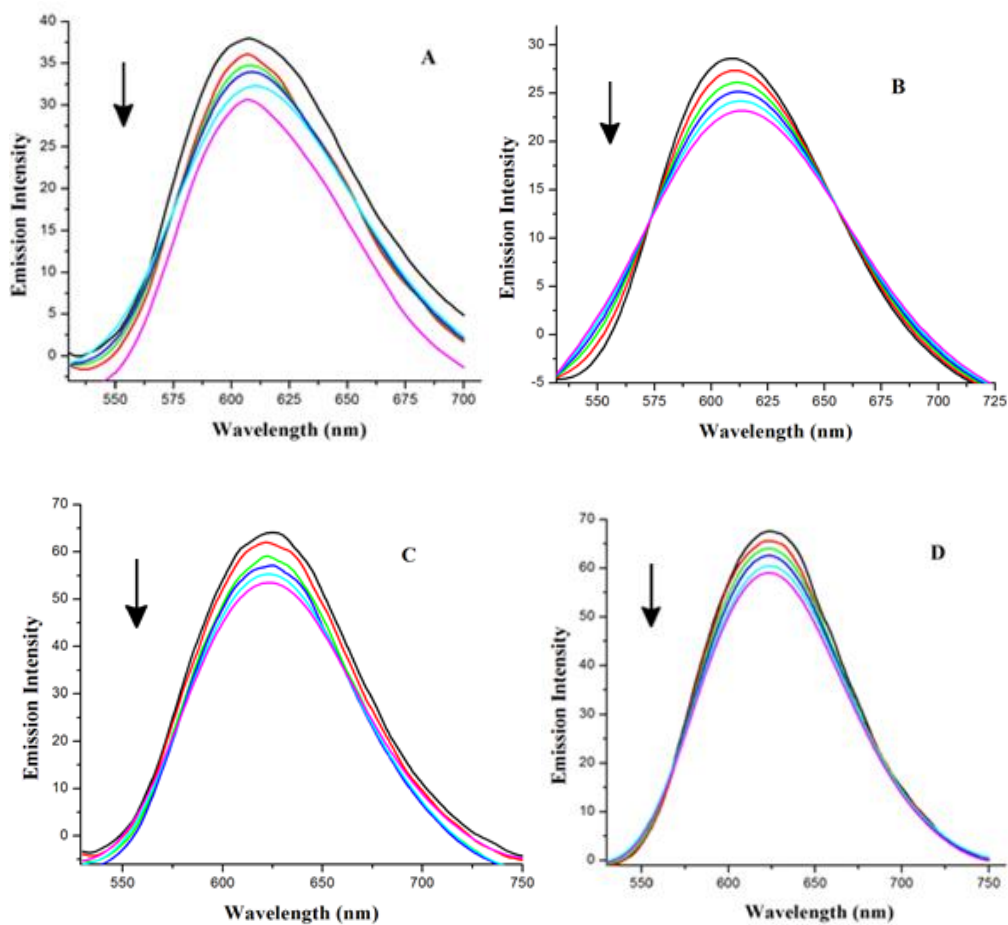

Figure 7. Emission titration of the DNA-EB system in the presence of compounds L_1 (A), L_2 (B), complex **1** (C) and complex **2** (D).
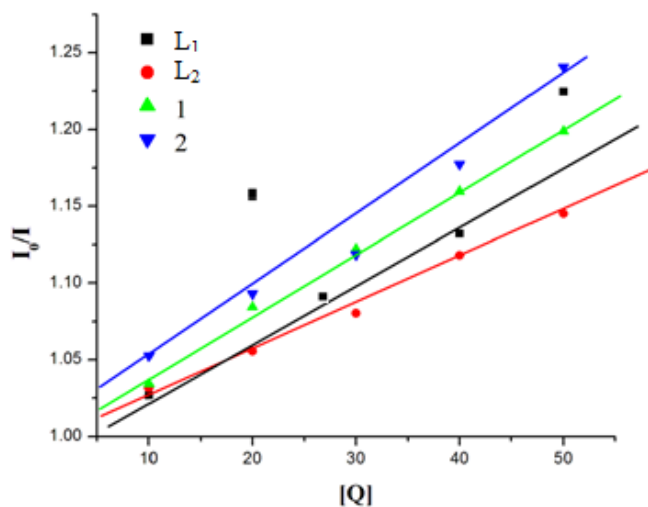
Figure 8. Stern-Volmer plot of the fluorescence titration for the compounds.

Viscosity experiment

In addition to the experiments carried out so far to find out the binding mode, viscosity measurements need to be carried out to confirm the mode of binding of the compounds [63]. Hence, we carried out the viscosity measurements in order to find out the relative change in viscosity of DNA in the presence of increasing amounts of complexes **1** and **2** which suggested that the viscosity of DNA increases on the addition of **1**and **2** (Figure 9). In general, the viscosity of DNA increases steadily when compounds intercalate between adjacent DNA base pairs, and hence, these results indicate that complexes **1** and **2** bind to CT-DNA by the intercalation mode and also that the complex **2** binds to CT-DNA more strongly than complex **1**.
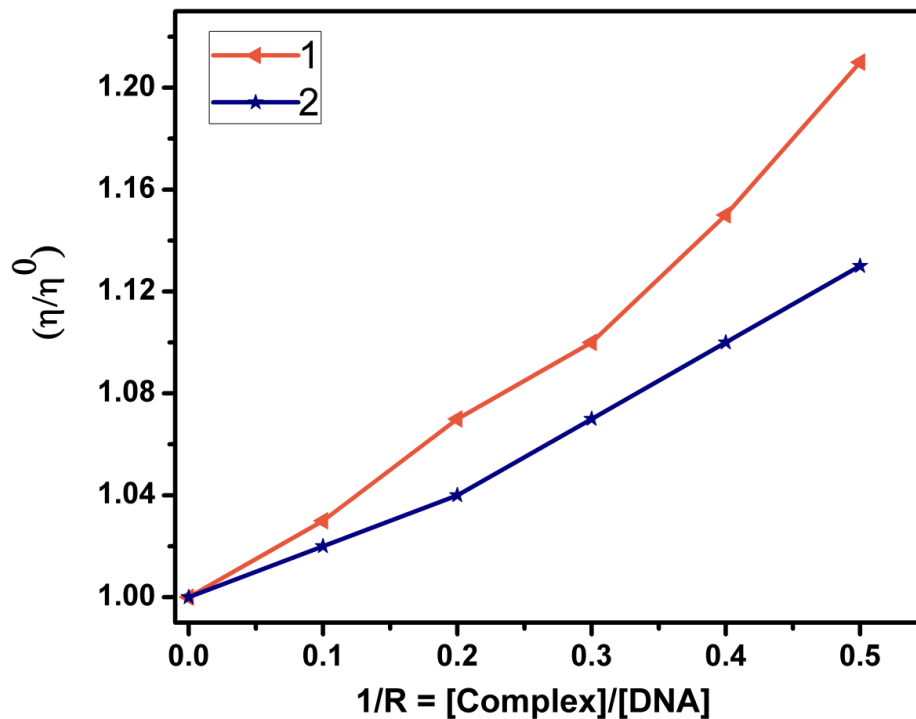
Figure 9. Viscosity of the complexes on the adding of CT-DNA.

Protein binding studies

Since proteins are involved in the transport of drugs through the bloodstream, it is also important to find out how the compounds interact with protein in order to assess their ability to function as a drug. Thus, it is essential to understand the protein–compound interaction and hence, binding experiments with BSA were carried out using the newly synthesized ligands and complexes through fluorescence spectral studies. The fluorescence spectra were recorded in the range of 290-450 nm upon excitation at 342 nm by adding various concentrations of the compounds (0-50 µM) to the solution of BSA (1 µM). The recorded fluorescence emission spectra of BSA are given in Figure 10. It is found from the spectra that there is hypochromicity with a blue shift for all the four compounds studied indicating that all the compounds bind to the BSA protein [64]. Further, fluorescence quenching data has also been examined with the Stern-Volmer equation and Scatchard equation. If the binding of compounds with BSA takes place at equilibrium, the equilibrium binding constant can be examined according to the Scatchard equation.

$$\log[I^0\text{-}I/I\,] = \log K_{bin} + n \log[\,Q]$$

where K_{bin} is the binding constant of the compoundsthrough BSA and n is the number of binding sites. One can calculate the binding constant (K_{bin}) and the number of binding sites (n) from the plot of $\log[F^0\text{-}F/F]$ *versus* $\log[Q]$ (Figure 11). Moreover, from the plot of I^0/I *versus* [Q], the quenching constant (Kq) have also been calculated (Figure 12). The calculated K_q, K_{bin}, and n values are listed in Table 2. The calculated value of n is nearly 1 for all of the compounds, indicating the presence of just a single binding site in BSA for all of the compounds [65,66]

Table 2. Quenching constant (K_q), protein binding constant (K_{bin}) and number of binding sites (n).

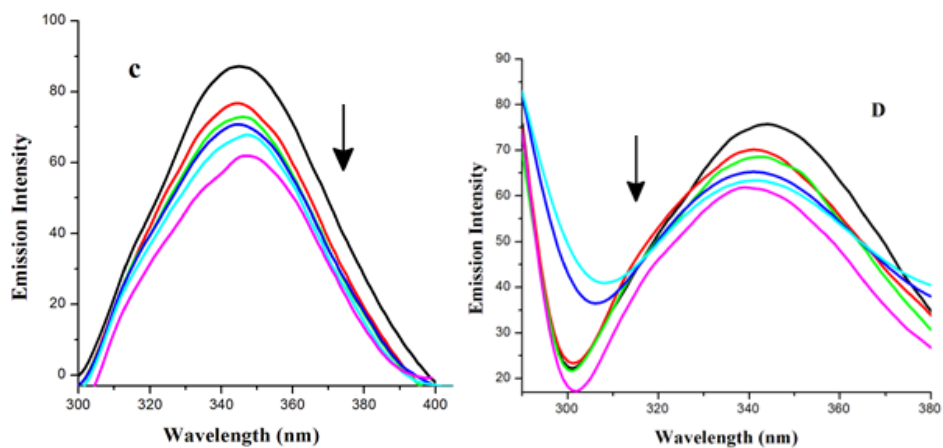| Compound	K_q (M^{-1})	K_{bin}(M^{-1})	n
L$_1$	1.17×10^2	6.41×10^3	0.59
L$_2$	2.96×10^3	1.89×10^2	0.76
1	2.06×10^4	8.13×10^3	1.10
2	3.88×10^3	2.77×10^2	0.79
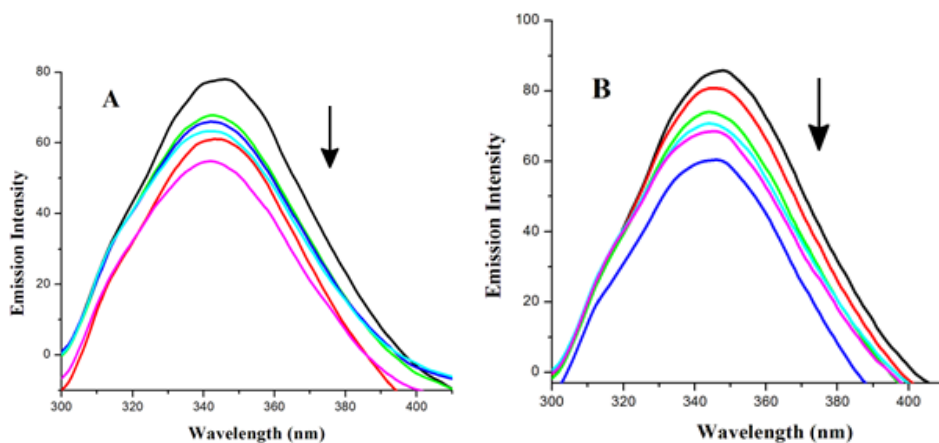
Figure 10. Fluorescence quenching curves of BSA in the absence and presence of compounds **L₁**(A), **L₂**(B), complex **1** (C) and complex **2** (D).
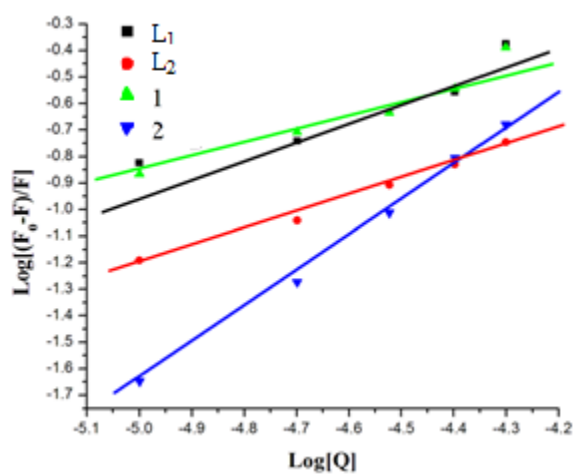

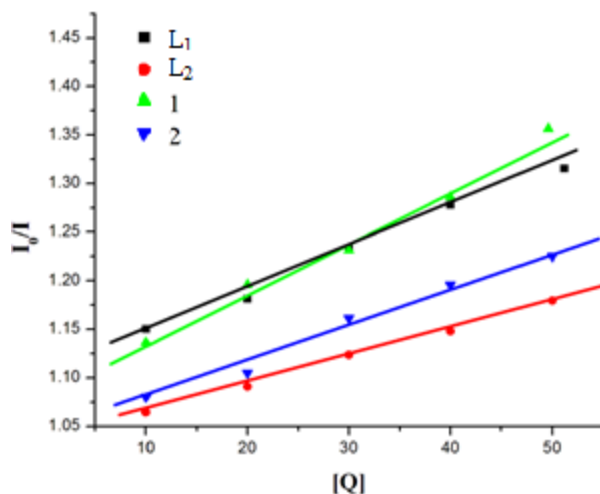**Figure 11**. Scatchard plot of the compounds with BSA.

Figure 12. Stern–Volmer plot of the compounds with BSA.

In order to find out the exact nature of the interaction of the new compounds with protein, UV absorption spectral titrations of BSA in the presence and absence of ligands and complexes have been carried out and the results are shown in Figure 13. It can be seen from the spectra that there is a decrease in the intensity of absorptionof BSA with the addition of the test compounds indicating clearly that a static interaction takes place between the test compounds and BSA [67].
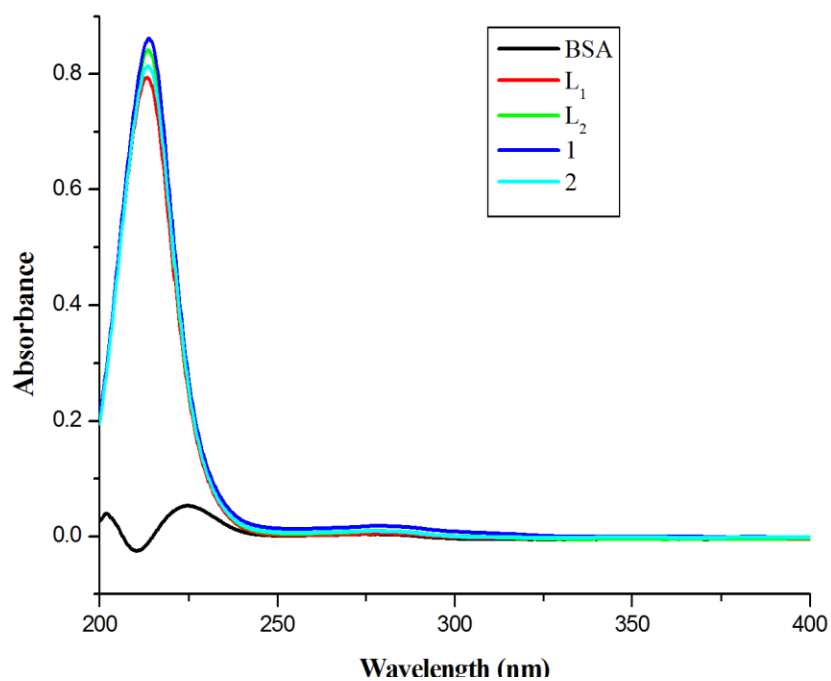

Figure 13. Absorption titrations of the compounds with BSA.

Cytotoxicity properties of the compounds

Significant information obtained from the interactions of the new compounds with both DNA and protein encouraged us to proceed further to investigate the *in vitro* cytotoxicity activity. A detailed study of the new compounds with PANC-1 and Hela cells were carried out with different concentration of synthesized compounds (**L₁**, **L₂**, **1** and **2**) incubated for 24 h, followed by incubation with WST-8 cell counting kit for 24 hours and the data are presented in Figures 14 and15. Complexes **1** and **2** showed significant cytotoxic properties against both PANC-1 and Hela cells when compared to the ligands. It can be seen that the Complex **1** showed potent activity at 11.67 µM (IC_{50}) while complex **2** showed activity at 16.41 µM (IC_{50}) in Hela cells. However, Complex 1 and 2 showed moderate activity against PANC-1 cells with IC_{50} of 17.91 and 25.13 µM, respectively.
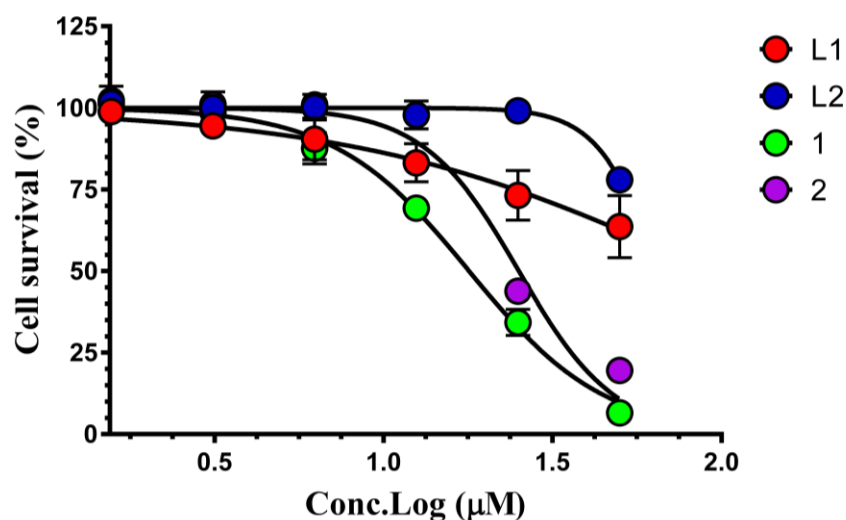

Figure 14. Effect of synthesized complexes (L₁, L₂, 1 and 2) against PANC-1cells. Data was calculated by mean±S.D with three replications. Positive control- Gemcitabine >25 µM.

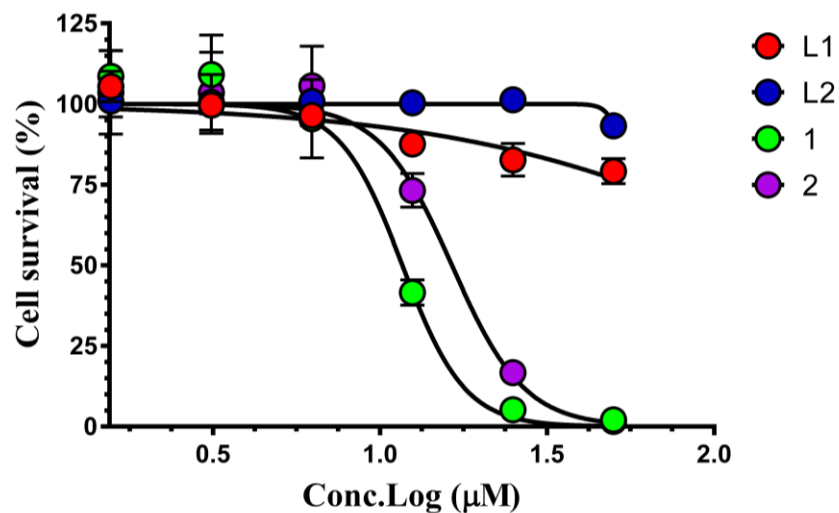**Figure 15**. Effect of synthesized complexes (L$_1$, L$_2$, 1 and 2) against Hela cells. Data was calculated by mean±S.D with three replications. Positive control- Paclitaxel 0.0014 µM.

Fluorescence study for apoptosis analysis

Finally, fluorescence imaging studies were carried out to determine the cell death mechanism of the compounds by using treated and untreated PANC-1 and Hela cells. The cells were incubated with EB/ AO for 5 min in the dark before an image was captured in EVOS FL cell imaging system (20 × objective). It was found that after treatment of complexes **1** and **2**, there was a dramatic increase in the apoptosis in both PANC-1 (50 µM) and Hela (25 µM) cells when compared to the control cells (green color fluorescence indicates live cells while a red color indicates dead cells) (Figure 16).The morphological changes examined by this staining method suggested that the cell death mechanism was through apoptosis.
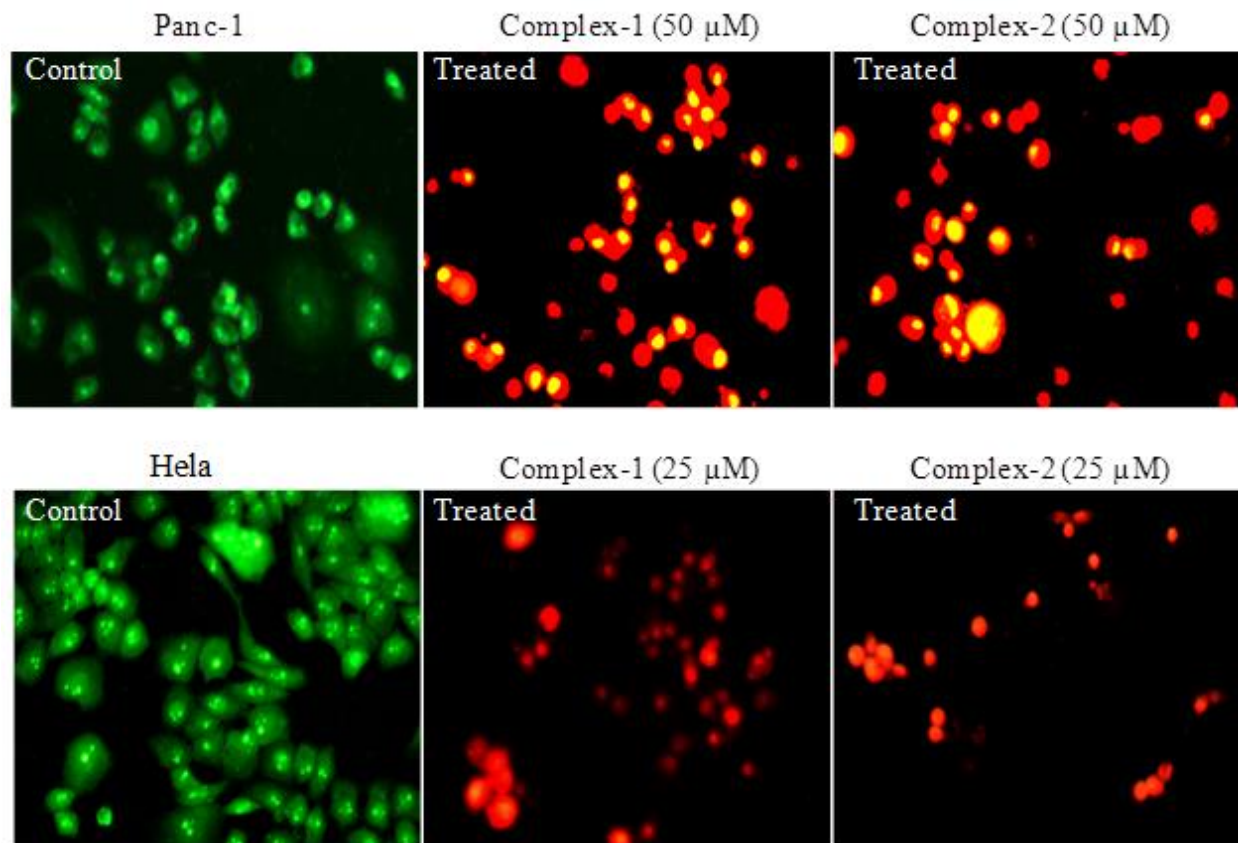
Figure 16. PANC-1 and Hela cells were treated with complex **1** and complex **2** and incubated at 24 h. Treated and untreated cells were stained with EB/AO. Images were taken by the fluorescent modes. Live cells were stained with AO and emission was captured by a bright green fluorescence. Dead cells were stained with EB and emission was captured by a red fluorescence (EVOS FL cell imaging system-20 × objective). Merged images of treated and control cells were presented.

Conclusion

Reactions of [CuCl$_2$(PPh$_3$)$_2$] with 3-methoxy-3-quinolin-3-ylimino-methyl-2-phenol and 4-methoxy-3-quinolin-3-ylimino-methyl-2-phenol yielded an one dimensional multinuclear and another mononuclear copper complexes. The molecular structures of the ligands and complexes have been confirmed by the single crystal X-ray diffraction method. The phenolic oxygen and azomethine nitrogen atom of the ligand coordinated to copper ion in a monobasic bidentate manner with approximately square planar geometry resulting in two different types of complexes, a polymeric and a mononuclear.It is quite surprising and difficult to explain how the

change in the position of methoxy in the ligand can lead to the formation of two types of complexes under a similar reaction conditions. Intercalative binding mode of the compounds with CT-DNAwas studied by absorption and emission titrations. Potential BSA interactions of the complexes were also examined by absorption and fluorescence quenching experiments, which indicate a strong interaction between the complexes and BSA by a static quenching mechanism. The *in vitro* cytotoxicity activities of the compounds were evaluated against PANC-1 and Hela cancer cell lines. Complex **1** and **2** displayed significant inhibitory effect on both the cell lines, specifically complex **1** showed potent activity at 11.67 µM against Hela after 24 h treatment. Morphological changes of the cells were confirmed by fluorescence imageusing EB/AO reagent. The strong binding affinity and cytotoxicity properties of the complex **1** might be due to the greater planar area, which is attributed to the extension of the π system of the intercalated complex **2**. These results could be used for better understanding of the biological interactions of novel multinuclear and mononuclear complexes.

References

1. (a) R.K. Hocking, E.I. Solomon, in Molecular Electronic Structures of Transition Metal Complexes, ed. D.M.P. Mingos, P. Day, J.P. Dahl, Springer, NY, USA, 142 (2012) 155; (b) R.H. Crabtree, The Organometallic Chemistry of the Transition Metals, John Wiley & Sons, 2011; (c) M. Shatruk, C. Avendano, K.R. Dunbar, in Prog. Inorg. Chem. ed. K.D. Karlin, John Wiley & Sons, NY, USA, 56 (2009)155; (d) R. Boca, A Handbook of Magneto Chemical Formulae, Elsevier, Amsterdam, 2012; (e) D.S. Nesterov J. Jezierska, O.V. Nesterova, A.J.L. Pombeiro, A. Ozarowski, Chem. Commun.50 (2014) 3431-3434.

2. (a) S. Mukherjee, P.S. Mukherjee, Acc. Chem. Res.46 (2013) 2556-2566. (b) D. Venegas-Yazigi, D. Aravena, E. Spodine, E. Ruiz, S. Alvarez, Coord. Chem. Rev. 254 (2010)2086-2095. (c) W. Plass, Coord. Chem. Rev. 253 (2009) 2286-2295.

3. J. Costamagna, J. Vargas, R. Latorre, A. Alvarado, G. Mena, Coord. Chem. Rev.119 (1992)67-88.

4. A. Togni, L.M. Venanzi, Angew. Chem. Int. Ed. Engl. 33 (1994) 497-526.

5. F. Fache, E. Schulz, M.L. Tommasino, M. Lemaire, Chem. Rev. 100 (2000) 2159-2232.

6. I. Kostova, Recent Pat. Anti-Cancer Drug Discovery1 (2006) 1-22.

7. B.P. Esposito, R. Najjar, Coord. Chem. Rev. 232 (2002) 137-149.

8. T.M. Sielecki, J.F. Boylan, P.A. Benfield, G.L. Trainor, J. Med. Chem. 43 (1999) 1-18.

9. Z. Zang, L. Jin, X. Qian, M. Wei, Y. Wang, J. Wang, Y. Yang, Q. Xu, Y. Xu, F. Liu, Chem. BioChem.8 (2007) 113-121.

10. P.K. M. Siu, D.L. Ma, C. M. Che, Chem. Commun. (2005) 1025-1027.

11. W.O. Foye, Cancer Chemotherapeutic Agents; American Chemical Society: Washington, DC, (1995).

12. S. Adsule, V. Barve, D. Chen, F. Ahmed, Q.P. Dou, S. Padhye, F.H. Sarkar, J. Med. Chem.49 (2006) 7242-7246.

13. M. Sebastian, V. Arun, P.P. Robinson, A.A. Varghese, R. Abraham, E. Suresh,K.K.M. Yusuff, Polyhedron29 (2010) 3014-3020.

14. S.A. Filimon, C.G. Hrib, S. Randoll, I. Neda, P.G. Jones, M. Tamm, Z. Anorg. Allg. Chem.636 (2010) 691-699.

15. A.G. Quiroga, C.N. Ranninger, Coord. Chem. Rev. 248 (2004) 119–133.

16. C.D. Fan, H. Su, J. Zhao, B.X. Zhao, S.L. Zhang, J.Y. Miao, Eur. J. Med. Chem. 45 (2010) 1438-1446.

17. I. Pal, S. Dutta, F. Basuli, S. Goverdhan, S.M. Peng, G.H. Lee, S. Bhattacharya, Inorg. Chem. 42 (2003) 4338-4345.

18. A.R. Cowley, J.R. Dilworth, P.S. Donnelly, E. Labisbal, A. Sousa, J. Am. Chem. Soc. 124 (2002) 5270-5271.

19. T.S. Lobana, S. Khanna, R.J. Butcher, A.D. Hunter, M. Zeller, Inorg. Chem. 46 (2007) 5826-5828.

20. J. Peisach, P. Aisen, The Biochemistry of Copper, ed. W. Blumberg, Academic Press, New York, (1966).

21. S. Banerjee, S. Mondal, W. Chakraborty, S. Sen, R. Gachhui, R.J. Butcher, A.M.Z. Slawin, C. Mandal, S. Mitra, Polyhedron28 (2009) 2785-2793.

22. C.D. Fan, H. Su, J. Zhao, B.X. Zhao, S.L. Zhang, J.Y. Miao, Eur. J. Med. Chem. 45 (2010) 1438-1446.

23. Y. Li, Z.Y. Yang, Inorg. Chim. Acta362 (2009) 4823-4831.

24. Z.C. Liu, B.D. Wang, Z.Y. Yang, Y. Li, D.D. Qin, T.R. Li, Eur. J. Med. Chem. 44 (2009)4477-4484.

25. D.S. Raja, N.S.P. Bhuvanesh, K. Natarajan, Eur. J. Med. Chem. 46 (2011) 4584-4594.

26. D. Senthil Raja, N.S.P. Bhuvanesh, K. Natarajan, Inorg. Chem. 50 (2011) 12852-12866.

27. Z.Q. Liu, M. Jiang, Y.T. Li, Z.Y. Wu, J.X. Yang, Inorg. Chim. Acta362 (2009) 1253-1259.

28. Y.T. Li, Z.Q. Liu, Z.Y. Wu, J. Inorg. Biochem. 102 (2008)1790-1797.

29. Z.Q. Liu, Y.T. Li, Z.Y. Wu, Y.L. Song, Inorg. Chim. Acta361 (2008) 226-232.

30. A.I. Vogel, Text Book of Practical Organic Chemistry, 5th *E*d. Longman. London, (1989).

31. S. Nayak, A.P. Colin, C. Seaton, P. Gamez, J. Reedijk, Polyhedron107 (2016) 172-175.

32. Dileep Ramakrishna, BadekaiRamachandraBhat, A catalytic process for the selective oxidation of alcohols by copper (II) complexes, Inorg. Chem. Comm. 14 (2011) 690-693.

33. S.K. Panja, N. Dwivedi, S. Saha, Tetrahedron Lett. 53 (2012) 6167-6172.

34. D. Senthil Raja, E. Ramachandran, N.S.P. Bhuvanesh, K. Natarajan, Eur. J. Med. Chem. 64 (2013) 148-159.

35. D.S. Raja, G. Paramaguru, N.S.P. Bhuvanesh, J.H Reibenspies, R. Renganathan, K. Natarajan, Dalton Trans.40 (2011) 4548-4559.

36. (a) J. Haribabu, K. Jeyalakshmi, Y. Arun, N.S.P. Bhuvanesh, P.T. Perumal, R. Karvembu, RSC Adv. 5 (2015) 46031-46049. (b)J. Haribabu, K. Jeyalakshmi, Y. Arun, N.S.P. Bhuvanesh, P.T. Perumal, R. Karvembu, J. Biol. Inorg. Chem.22 (2017) 461-480. (c) M. Muralisankar, J. Haribabu, N.S.P. Bhuvanesh, R. Karvembu, A. Sreekanth, Inorg. Chim. Acta449 (2016) 82-95.

37. (a) K. Jeyalakshmi, J. Haribabu, N.S.P. Bhuvanesh, R. Karvembu, Dalton Trans.45 (2016) 12518-12531.(b) J. Haribabu, G.R. Subhashree, S. Saranya, K. Gomathi, R. Karvembu, D. Gayathri, J. Mol. Struct. 1110 (2016) 185-190. (c) J. Haribabu, G.R. Subhashree, S. Saranya, K. Gomathi, R.Karvembu, D. Gayathri, J. Mol. Struct.1094 (2015) 281-291.

38. Bruker, SAINT+ Integration Engine, Data Reduction Software, Bruker Analytical X-ray Instruments Inc., Madison, WI, USA,(2007).

39. Bruker, SADABS, Bruker AXS area detector scaling and absorption correction, Bruker Analytical X-ray Instruments Inc.*,* Madison, Wisconsin, USA,(2001).

40. L. Palatinus, G. Chapuis, J. Appl. Crystallogr.40 (2007) 786-790.

41. L. Palatinus, S.J. Prathapa, S. van Smaalen, J. Appl. Crystallogr.45 (2012) 575-580.

42. G.M. Sheldrick, Acta Crystallogr., Sect. A: Found. Crystallogr. 64 (2008) 112-122.

43. G.M. Sheldrick, Acta Crystallogr.C7 (2015) 13-8.

44. O.V. Dolomanov, L.J. Bourhis, R.J. Gildea, J.A.K. Howard, H. Puschmann, J. Appl. Crystallogr.42 (2009) 339-341.

45. A.L. Spek, J. Appl. Crystallogr.36 (2003) 7-13.

46. A L. Spek, Acta Crystallographica Section D-Biological Crystallography65 (2009) 148-155.

47. B.S. Creaven, E. Czegledi,M. Devereux,E. Enyedy,A. Foltyn-Arfa Kia,D. Karcz,A.K.S. McClean,N.V. Nagy,Andy Noble,A. Rockenbauer,T. Szabo-Planka, M. Walsh, Dalton Trans. 39 (2010) 10854-10865.

48. P.M. Krishna, K.H. Reddy, Inorg. Chim. Acta362 (2009) 4185-4190.

49. Saswati, R. Dinda, C.S. Schmiesing, E. Sinn, Y.P. Patil, M. Nethaji, H. Stoeckli-Evans, R. Acharyya, Polyhedron50 (2013) 354-363.

50. A.B.P. Lever, Inorganic Electronic Spectroscopy, Second Ed. Elsevier, Amsterdam.

51. G. Ayyannan, M. Mohanraj, G. Raja, N. Bhuvanesh, R. Nandhakumar, C. Jayabalakrishnan, Inorg. Chim. Acta453 (2016) 562-573.

52. F. Basuli, M. Ruf, C.G. Pierpont, S. Bhattacharya, Inorg. Chem.37 (1998) 6113-6116.

53. L.M. Fostiak, I. Gracia, J.K. Swearinger, E. Bermejo, A. Castineivas, D.X. West, Polyhedron22 (2003) 83-92.

54. R. Loganathan, S. Ramakrishnan, E. Suresh, A. Riyasdeen, M.A. Akbarsha, M. Palaniandavar, Inorg. Chem. 51 (2012)5512-5532.

55. T.M. Klapotke, C.M. Sabate, J. Stierstorfer, Z. Anorg, Allg. Chem. 634 (2008)1867-1874.

56. Z.C. Liu, B.D. Wang, Z.Y. Yang, Y. Li, D.D. Qin, T.R. Li, Eur. J. Med. Chem. 44 (2009)4477-4484.

57. Q.L. Zhang, J.G. Liu, H. Chao, G.Q. Xue, L.N. Ji, J. Inorg. Biochem. 83 (2001) 49-55.

58. D. Senthil Raja, N.S.P. Bhuvanesh, K. Natarajan, Eur. J. Inorg. Chem. 47 (2012) 73-85.

59. F.J. Meyer-Almes, D. Porschke, Biochemistry32 (1993) 4246-4253.

60. G.M. Howe, K.C. Wu, W.Bauer, Biochemistry 19 (1976) 339-347.

61. Y.B. Zeng, N. Yang, W.S. Liu, N. Tang, J. Inorg. Biochem. 97 (2003) 258-264.

62. Y. Hu, Y. Yang, C. Dai, Y. Liu, X. Xiao, Biomacromolecules11(2010) 106-112.

63. K. Jeyalakshmi, J. Haribabu, C. Balachandran, N.S.P. Bhuvanesh, N. Emi, R. Karvembu, New J. Chem. 41 (2017) 2672-2686.

64. D.S. Raja, G. Paramaguru, N.S.P. Bhuvanesh, J.H. Reibenspies, R. Renganathan, K. Natarajan, Dalton trans. 40 (2011) 4548-4559.

65. D.S. Raja, N.S.P. Bhuvanesh, K. Natarajan, Eur. J. Med. Chem. 46 (2011) 4584-4594.

66. A. Sulkowska, J. Mol. Struc, 616 (2002) 227-232.

67. E. Ramachandran, D. Senthil Raja, N.P. Rath, K. Natarajan, Inorg. Chem. 52 (2013) 1504-1514.